Artery and vein segmentation on brain CTA using CTP for contrast-phase augmentation

Henk van Voorst[1,2], Daniel de Wilde[1], Pere Canals[1,2], Maya Schwartz[1,2], Jamie Kesten[1,2], Praneeta Konduri[2,3], Aroosa Zamarud[1,2], Bin Jiang[1], Soren Christensen[1,2,3], Donghoon Kim[1], Yongkai Liu[1], Greg Albers[2,3], Gagan Sharma[3], Mark Parsons[3], Greg Zaharchuk[1], and Maarten Lansberg[2,3] Jeremy Heit[1,2]

[1] Department of Radiology, Stanford University School of Medicine, Palo Alto, USA
[2] Stanford Stroke Center, Stanford University School of Medicine, Palo Alto, USA
[3] Department of Neurology Stanford University, School of Medicine, Palo Alto, USA
[4] Department of Neurology, University New South Wales, Syndey, Australia

Abstract. Detailed automated artery and vein segmentation on brain CT angiography (CTA) enables the use of standardized quantitative collateral scores for prognosticating outcomes to support treatment decisions in acute ischemic stroke. However, current deep learning methods for vessel segmentation are inaccurate for small vessels, fail to separate arteries and veins, do not account for variations in contrast bolus timing, and require laborious manual annotations. To address these issues, we developed a deep learning method to separate intracranial artery and vein segmentation from semi-automatically annotated thin-slice CT perfusion (CTP) source data. These CTPs were used to simulate CTAs with variable contrast timing, thereby enabling contrast-phase augmentation during training. We compared models trained with and without contrast-phase augmentation and evaluated replicability across models trained from scratch and fine-tuned foundation models. Segmentation volumes in either hemisphere were used to automatically measure arterial and venous quantitative collateral scores (aQCS/vQCS) that were compared to expert-rated Tan scores (0-3) and cortical vein opacification scores (COVES; 0-6). Across external test sets of simulated and real CTAs, contrast-phase augmentation improved artery and vein segmentation performance for models trained from scratch, but yielded only a limited or no gain for foundation models. Models trained from scratch outperformed fine-tuned foundation models. aQCS and vQCS showed high agreement with expert rater scores. Our results demonstrate the quantitative benefits and clinical utility of contrast-phase augmentation for deep-learning-based artery and vein segmentation.

Keywords: Segmentation · Ischemic Stroke · Artery · Vein · Collaterals

1 Introduction

Automated segmentation of intracranial arteries and veins on brain single-phase CT angiography (CTA) can improve the diagnosis, characterization, and prog-

nosis of neurovascular diseases [8, 3, 12]. In acute ischemic stroke, arterial and venous collaterals indicate distortions in blood inflow and outflow and are therefore prognostic for infarct expansion and patient outcomes [12, 1]. Radiologist-based ordinal ratings of the Tan score for arteries and the cortical vein opacification score (COVES) for veins on brain CTA are considered for prognostication and treatment decisions, but have suboptimal interrater agreement [24, 1]. To enable objective quantification of the collateral circulation, quantitative collateral scores (QCS, arterial: aQCS, venous: vQCS) compare the volume of vessel segmentations between the infarcted and contralateral hemispheres[3, 24]. As QCS relies on vessel segmentations, there is a strong need for accurate automated distal artery and vein segmentation methods.

Supervised deep learning has improved automated vessel segmentation methods for various imaging modalities and organs [4, 8]. However, due to the lack of laborious reference segmentations, separate artery and vein segmentation on brain CTA remains challenging. Most brain CTA vessel segmentation methods and public datasets focus on segmenting arteries only [5, 9, 26], do not distinguish between arteries and veins [5, 9, 17, 19, 18], or limit evaluation to larger vessels, and neglect smaller distal vessels [5, 9, 26]. Furthermore, variations in vascular contrast opacification across CTAs significantly affect the performance of vessel segmentation methods but are not accounted for in model development. In contrast to CTA, detailed artery and vein segmentations can be acquired using CT perfusion (CTP) source data [13]. CTP consists of a temporal sequence of low-dose CTAs acquired while contrast is flowing through the brain. Meijs et al. exploited the spatiotemporal characteristics of CTP for detailed deep learning-based artery and vein segmentation [13]. These gains in CTP source data have not been translated into improved artery and vein segmentation on brain CTA.

Image augmentation techniques are used during training to obtain feature representations of deep learning models that are robust to variations in image orientation and quality [7]. Conventional augmentation procedures that improve performance on CT and MR imaging tasks include filtering techniques, such as blurring and sharpening, adding noise, rotation, and flipping [7, 20]. More recently, generative deep learning methods have been proposed to generate or augment input training data to enhance deep learning tasks [23, 7]. Conventional and generative deep learning augmentation techniques have improved vessel segmentation on a variety of modalities and organs [7, 20, 23], but these methods may not fully represent realistic variations in CTAs. Provided that intravascular contrast attenuation differences between CTAs can be considerable and affect the quality of separate artery and vein segmentation, contrast-phase augmentation may improve deep learning-based segmentation of arteries and veins.

To mitigate the effects of brain CTA contrast-phase timing differences on artery and vein segmentation, we propose training segmentation models using contrast-phase-augmented CTAs. We achieve contrast-phase augmentation by simulating CTAs with varying acquisition timings from CTP source data. Additionally, the use of simulated CTAs improves manual reference segmentation quality and reduces the annotation burden by enabling semi-automated artery and vein seg-

mentation techniques available for CTP [13].
The contributions of this study are as follows: 1) We present the first deep learning model for separate artery and vein segmentation on brain CTA. 2) We prove that vessel segmentation models trained on CTAs simulated from CTP source data also result in high-quality artery and vein segmentations on real CTAs. 3) We show that contrast-phase augmentation based on simulated CTAs improves artery and vein segmentation performance. 4) We show that our segmentations result in high agreement of aQCS with Tan and vQCS with COVES. 5) We present our vQCS as the first automated brain CTA venous outflow scoring method. Our models' artery and vein segmentation performances are validated on external datasets of simulated CTAs and real CTAs. QCSs are evaluated in a reader study conducted on a large external retrospective cohort.

2 Methods

Our method leverages the similarity between CTP and CTA and assumes that deep learning segmentation models trained on CTP-simulated CTAs can be directly transferred to real CTAs. Traditionally, CTP has been used to compute perfusion maps of brain tissue using singular value decomposition of changes in tissue contrast attenuation relative to an arterial input function (AIF) of a large intracranial artery [6]. For this study, we focus on CTP source data for simulating multi-phase CTA sequences and do not consider perfusion maps. Figure 1 visually describes our methods.

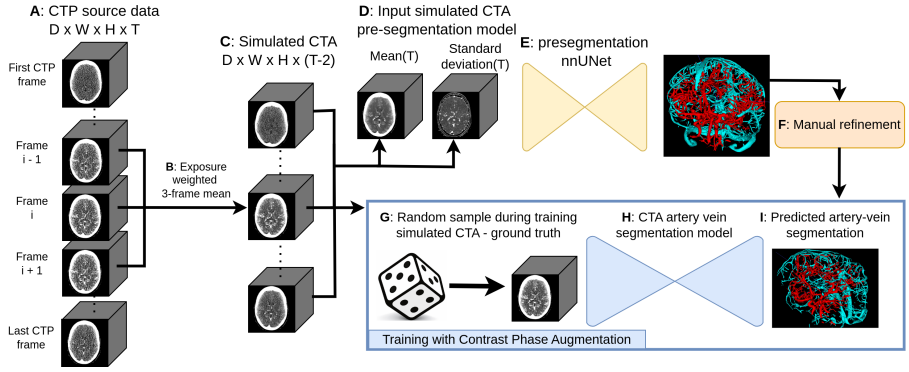

Fig. 1. Graphical methods description. Spatiotemporal CTP source data (A) is converted by taking three-frame exposure weighted means (B) to generate simulated CTAs (C). Temporal mean and standard deviation images of the spatiotemporal sequence (D) serve as input for an nnUNet artery-vein pre-segmentation model (E), segmentations are manually refined (F). Simulated CTAs are randomly sampled (G) to train a CTA segmentation model (H) for artery-vein segmentation (I).

2.1 Simulating CTA from CTP source data

CTP source data consists of a four-dimensional spatiotemporal sequence – depth: D, height: H, width: W, time: T – of low-dose CTAs acquired while intravenously injected contrast fluid is flowing through arteries and veins (Figure 1A). Due to the lower-dose exposure of CTP frames, quantum noise levels are higher than those of higher-exposure real CTAs, resulting in lower signal-to-noise levels [14]. To alleviate this CTP-CTA discrepancy and account for exposure variations across frames, we apply an exposure-weighted filter to each CTP frame (i) using the preceding ($i-1$) and subsequent ($i+1$) frames to simulate CTAs. Following [14], exposures of current E_i, preceding E_{i-1}, and subsequent E_{i+1} frames are used to obtain a frame specific exposure weight $\omega_i = \frac{E_i}{E_{i-1}+E_i+E_{i+1}}$. Exposure weights ω_i are applied to each 3D CTP frame in the temporal sequence $I_{D,W,H,i}$. Simulated CTAs $\tilde{I}_{D,W,H,i}$ are acquired by summing three subsequent exposure weighted frames $\tilde{I}_i = \sum_{j=i-1}^{i+1} \omega_j I_j$, thereby acquiring an exposure weighted mean (Figure 1B). As a result of using preceding and subsequent frames for exposure weighted filtering, the first and last CTP frames are not considered for generating simulated CTAs and thus the total length of the sequence becomes shorter $T-2$. The simulated CTAs are linearly interpolated across time to generate a sequence with 2-second intervals that closely matches the original CTP acquisition protocol (Figure 1C).

2.2 Semi-automated CTP reference segmentation

As the simulated CTA sequence incorporates temporal contrast attenuation, it becomes easier to distinguish vessels from dense tissues such as bone and cartilage. Furthermore, temporal contrast attenuation changes enhance the separation of arteries and veins. We exploit these temporal attenuation changes by using the mean and standard deviation of contrast density across time (Figure 1D). Manual artery-vein reference segmentations are refined by inspecting contrast attenuation changes in varying simulated CTA timeframes. To expedite the annotation process, we train an nnUNet [11] on 10 manually annotated simulated CTA sequences for automated artery and vein segmentation (Figure 1E). The nnUNet achieves a mean 5-fold cross-validation Dice of 0.81. This model is used to acquire presegmentations for all simulated CTA sequences. Presegmentations are subsequently manually refined by inspecting consecutive simulated CTA frames (Figure 1F).

2.3 Contrast-phase augmentation

Using our simulated CTA sequence, we can determine the 'true' peak arterial phase and iteratively select frames at varying time intervals relative to the peak to train segmentation models. We refer to this iterative sampling of simulated CTAs relative to the 'true' peak arterial phase as contrast-phase augmentation. To determine the arterial peak in the simulated CTA sequence, we analyze the contrast attenuation curve of a seed point – sized 3x3x3 voxels – in the terminal

internal carotid artery or the M1 segment of the middle cerebral artery. The simulated peak arterial CTA ($t = 0$) is determined 2 seconds after the seed points' attenuation peak, as distal arteries and veins exhibit a delay in peak attenuation relative to proximal large arteries. For contrast-phase augmentation, we randomly selected simulated CTAs between -6 and +6 seconds from the arterial peak with 2-second intervals (Figure 1G) to train deep learning models trained for artery and vein segmentation (Figure 1H-I). Models trained without contrast-phase augmentation receive only the simulated peak arterial CTA ($t = 0$).

3 Experiments and Results

3.1 Datasets and evaluation metrics

We retrospectively collected 44 CTP source scans for training from a single center (male/female: 24/20, age median[IQR]: 79[68;83] years, baseline NIHSS median[IQR] : 9[6;14], Tan collateral score 0/1 or 2/3: 15/10/19, occlusion location M1/M2/ PCA/ACA/no occlusion: 14/5/13/7/5). Between June and July 2024, we prospectively collected 17 CTP source data scans from a second institution to convert into simulated CTAs for external testing (male/female: 9/8, age median [IQR]: 56[50;67], diagnosis no acute ischemic/chronic ischemia/small infarct/ICA occlusion/intercranial hemorrhage: 10/2/2/2/1). 20 real CTAs from patients with a large vessel occlusion were retrospectively included from a multicenter cohort study [25] male/female: 11/9, (age median[IQR]: 74[61;81] years, baseline NIHSS median[IQR]: 14[9;19], Tan collateral score 0/1/2/3: 2/7/7/4, occlusion location M1/M2/ICA/M3 or ACA: 11/4/3/2). Arteries and veins were annotated in the simulated CTA sequence (section 2.2). For Real CTAs, arteries and veins were manually annotated using 3D Slicer. Manual refinement of automated simulated CTA segmentations and manual from-scratch segmentation of real CTAs were performed by one trained rater (2 years of experience), refined by a second experienced rater (6 years of experience), and finalized by a board-certified interventional neuroradiologist (15+ years of experience). We only included CTPs and real CTAs with a slice thickness of $\leq 1mm$. For evaluation, we considered only intracranial arteries and veins selected using a manually adjusted brain and skull mask [22], beginning at the brainstem. Artery and vein segmentation performance was evaluated qualitatively by inspecting 3D segmentation renderings and quantitatively using the voxelwise Dice coefficient (Dice) and centerline Dice (clDice), reporting mean with standard errors ($mean \pm se$). Simulated CTAs performance represents the mean performance of 7 frames ranging from -6 to +6 seconds.

3.2 Implementation details

We adapted the nnUNet (version 2.4.1) framework to train artery and vein segmentation models, with and without contrast-phase augmentation, using 5-fold cross-validation. Default nnUNet image augmentations were used for all

experiments: rotation, scaling, elastic deformation, flipping, cropping, and various intensity changes [11]. The following model architectures were trained from scratch: the original nnUNet implementation (nnUNet-org) [11], nnUNet with residual skip connections (nnUNet-RencL, nnUNet large setting) [10], and MedNeXt [16] (nnUNet large kernel setting). To leverage rich feature representations available from large-scale pretrained foundation models, we additionally evaluate fine-tuned foundation models: Merlin [2], CTFM [15], vessel segmentation foundation model (VFM) [23], and the Segment Anything Model for 3D medical imaging (SAM3D) [21]. We compare our methods with a previously reported supervised artery segmentation method by Canals et al. [5], which was trained on 162 CTAs from an independent uni-centric dataset and focused on large cerebral arteries. All models used identically splitted folds and were optimized for equally weighted cross-entropy and dice-loss. We used fixed patch sizes of 128x128x128 with a resampled spacing of 0.43, 0.43, 0.5 (HxWxD), corresponding to the median spacing of the training data scans, and a batch size of 2. Models that were trained with randomly initialized weights (from scratch) used a starting learning rate of 0.01 that was linearly decreased to 1e-5 over 1000 epochs with a stochastic gradient descent optimizer (Betas: 0.9 and 0.999, weight decay 3e-5). Foundation models were fine-tuned with an initial learning rate of 3e-5, reduced to 1e-5 over 500 epochs using a cosine annealing schedule with an AdamW optimizer (weight decay=0.01). Source code is available: github.com/anonymized.

3.3 Contrast-phase augmentation across models

Table 1 describes the Dice and clDice performance on two external test sets of 3 models trained from scratch and 4 fine-tuned foundation models trained with (w) and without (w/o) contrast-phase augmentation. Contrast-phase augmentation improved artery and vein segmentation performance, with greater effects in the models with the highest performance (nnUNet-org and nnUNet-RencL) and less benefits for foundation models (Merlin, VFM). Models trained from scratch outperform fine-tuned foundation models. The performance of CTFM and SAM3D was considerably lower than that of other models and did not benefit from contrast-phase augmentation. Figure 2 visualizes accurate and inaccurate segmentation predictions from nnUNet-org, trained with and without contrast-phase augmentation. Visual inspection of segmentation errors shows that contrast-phase augmentation improved segmentation of the internal carotid artery near the skull, in areas with low contrast opacification such as venous sinuses, and in more distal arteries and veins. Most segmentation errors were due to a limited degree of undersegmentation of large vessels and incorrect assignments of arteries as veins, or vice versa.

3.4 Ablation study: contrast-phase augmentation protocols

We evaluated the effect of variations in contrast-phase augmentation protocols during training on segmentation performance using the nnUNet-org method.

Table 1. Artery and vein segmentation performance for models trained with (w) and without (w/o) contrast-phase augmentation.

Task	Model	Simulated CTA				Real CTA			
		Dice		clDice		Dice		clDice	
		w	w/o	w	w/o	w	w/o	w	w/o
Artery	nnUNet-org	**69 ±2**	64 ±2	**71 ±2**	66 ±2	**77 ±1**	71 ±1	**80 ±1**	76 ±1
	nnUNet-RencL	68 ±2	64 ±2	**71 ±2**	65 ±2	**77 ±1**	72 ±1	**80 ±1**	76 ±1
	MedNeXt	63 ±2	61 ±2	67 ±2	65 ±1	69 ±1	68 ±2	74 ±2	72 ±2
	Merlin	59 ±2	56 ±2	62 ±2	56 ±2	73 ±1	72 ±1	78 ±1	75 ±1
	VFM	64 ±2	62 ±2	68 ±2	64 ±2	71 ±1	71 ±1	76 ±1	75 ±1
	CTFM	60 ±2	63 ±2	65 ±2	64 ±2	68 ±1	73 ±1	75 ±1	76 ±1
	SAM3D	54 ±2	58 ±2	54 ±2	56 ±2	60 ±1	66 ±1	62 ±2	65 ±1
	Canals et al. (2023)	NA	37 ±2	NA	29 ±1	NA	44 ±1	NA	39 ±1
Vein	nnUNet-org	**71 ±3**	67 ±3	68 ±2	**70 ±2**	**85 ±1**	81 ±2	**77 ±2**	75 ±3
	nnUNet-RencL	70 ±3	67 ±3	68 ±2	69 ±2	**85 ±1**	82 ±2	**77 ±2**	75 ±2
	MedNeXt	69 ±3	65 ±3	67 ±2	67 ±2	82 ±2	74 ±3	75 ±3	67 ±3
	Merlin	59 ±3	56 ±3	56 ±3	54 ±3	83 ±1	83 ±1	76 ±2	74 ±2
	VFM	69 ±3	66 ±3	66 ±2	65 ±2	82 ±2	81 ±2	75 ±2	74 ±3
	CTFM	65 ±3	66 ±3	67 ±2	66 ±2	71 ±4	81 ±2	69 ±4	75 ±3
	SAM3D	61 ±2	64 ±2	50 ±2	55 ±2	70 ±3	78 ±1	56 ±3	63 ±2

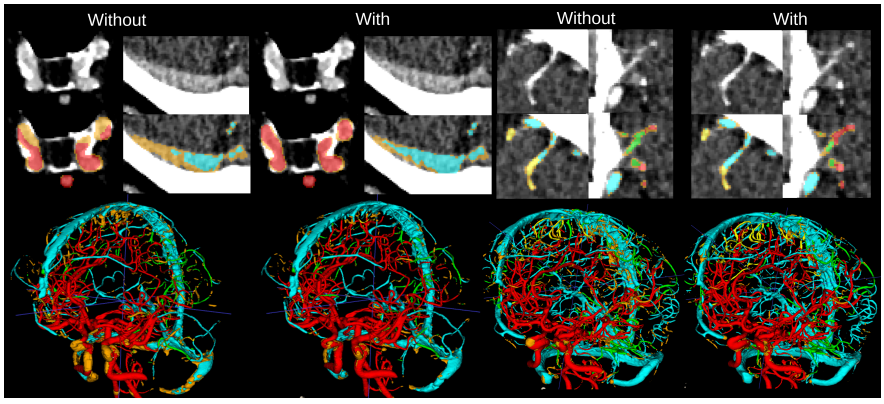

Fig. 2. Segmentation performance with and without contrast-phase augmentation. Contrast-phase augmentation-trained models visually improve artery and vein segmentation quality (fewer false negatives) near the skull (Left) and improve the separation of arteries from veins (Right). Red: true positive artery, Blue: true positive vein. Orange: false negative. Yellow: vein predicted as artery. Green: artery predicted as vein.

Figure 3 A/B show the Dice for artery and vein segmentation in the Real CTA test set using the standard protocol without (w/o) contrast-phase augmentation and protocols using additional simulated CTAs separate or combined 2, 4, and 6 seconds before and after the peak arterial phase. Any contrast-phase augmentation improved performance compared to w/o. The use of more extreme time differences to the arterial peak and combinations of time differences further enhanced Dice.

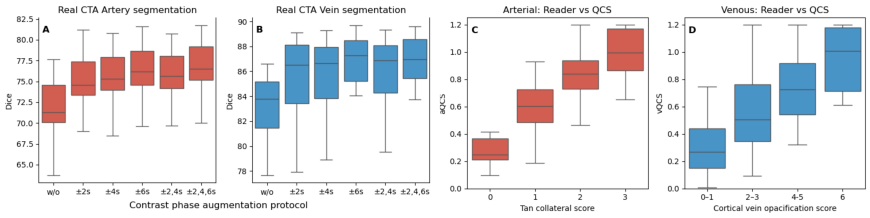

Fig. 3. A/B: Artery and vein segmentation performance for contrast-phase augmentation ablation study. C/D: Agreement of reader-based evaluation with arterial and venous quantitative collateral scores (aQCS/vQCS)

3.5 Quantitative Collateral Scoring

To evaluate the potential clinical use of artery and vein segmentations, we compare the agreement between quantitative collateral scores (QCS) and expert reader-based scores (Tan and COVES), which play a pivotal role in outcome prognostication in acute ischemic stroke. Reader-based arterial (Tan) and venous (COVES) scores assess specific vascular regions affected by ischemic stroke, while our segmentations cover the entire brain. For fair comparison, we restricted artery-vein segmentations for calculating arterial and venous quantitative collateral scores (aQCS/vQCS) to the corresponding Tan and COVES regions using atlas-based masks. We evaluate agreement using Spearman's correlation and test its significance using the Jonckheere-Terpstra test (JT). Figure 3 C/D shows the agreement QCS with reader-based scores for CTAs from 309 patients included from a multicenter prospective cohort. QCS below one indicates fewer vessels compared to the contralateral hemisphere; QCS above one indicates more vessels compared to the contralateral hemisphere. We observed a Spearman correlation between aQCS and Tan of 0.65 (JT-p<1e-5) and between vQCS and COVES of 0.57 (JT-p<1e-5).

4 Conclusion

In this study, we present a framework for contrast-phase augmentation to improve the training of deep learning segmentation models for intracranial artery

and vein segmentation on brain CTAs. Our contrast-phase augmentation method uses CTP source data to simulate CTAs with varying acquisition times relative to the peak arterial phase. Besides gains in deep learning-based segmentation quality, the use of simulated CTAs further improves and expedites detailed segmentation of arteries and veins. Due to semi-automated acquisition of reference segmentations, the proposed method scales well to larger datasets. On two external test sets of simulated and real CTAs, we show that contrast-phase augmentation improves segmentation quality across a variety of models trained from scratch but has a less profound impact on worse-performing fine-tuned foundation models. This study presents the first automated method for separating artery and vein segmentation on brain CTA. Although direct comparisons with other methods are complicated by dataset-specific variations, the Dice and clDice scores of our models trained with contrast-phase augmentation suggest that we approach state-of-the-art vessel segmentation performance [17, 9, 19, 18, 8, 4]. Lastly, we demonstrate that quantitative collateral scores derived from automated artery and vein segmentations show agreement comparable to expert-based scoring, reaching levels similar to interrater agreement among human raters [24]. Thus, we show the clinical utility of separate artery and vein segmentation using deep learning.

Disclosure of Interests. Henk van Voorst received funds from the Dutch Research Council (NWO-ZonMw) to conduct this research. Jeremy Heit is a consultant for Medtronic and Microvention. He is an advisory board member for MicroVention and iSchemaView.

References

1. Barghash, M., Salim, H.A., Mei, J., Tantawi, M., Elnaeem, A.K., Frade, H.C., Kabeel, K., Lakhani, D.A., Koneru, M., Hillis, A.E., others: Role and prognostic implications of venous outflow assessment in acute ischemic stroke. Journal of Neuroimaging **35**(1), e13256 (2025)
2. Blankemeier, L., Cohen, J.P., Kumar, A., Van Veen, D., Gardezi, S.J.S., Paschali, M., Chen, Z., Delbrouck, J.B., Reis, E., Truyts, C., others: Merlin: A vision language foundation model for 3d computed tomography. Research Square pp. rs–3 (2024)
3. Boers, A., Barros, R.S., Jansen, I., Berkhemer, O., Beenen, L., Menon, B.K., Dippel, D., van der Lugt, A., van Zwam, W., Roos, Y., others: Value of quantitative collateral scoring on CT angiography in patients with acute ischemic stroke. American journal of neuroradiology **39**(6), 1074–1082 (2018)
4. Bukenya, F., Bai, L., Kiweewa, A.: A Review of Blood Vessel Segmentation Techniques. 1st International Conference on Computer Applications and Information Security, ICCAIS 2018 pp. 1–10 (2018). https://doi.org/10.1109/CAIS.2018.8441989, iSBN: 9781538644263
5. Canals, P., Balocco, S., Díaz, O., Li, J., García-Tornel, A., Tomasello, A., Olivé-Gadea, M., Ribó, M.: A fully automatic method for vascular tortuosity feature extraction in the supra-aortic region: unraveling possibilities in stroke treatment planning. Computerized Medical Imaging and Graphics **104**, 102170 (2023)

6. Dehkharghani, S., Bammer, R., Straka, M., Albin, L., Kass-Hout, O., Allen, J., Rangaraju, S., Qiu, D., Winningham, M., Nahab, F.: Performance and predictive value of a user-independent platform for CT perfusion analysis: threshold-derived automated systems outperform examiner-driven approaches in outcome prediction of acute ischemic stroke. American Journal of Neuroradiology **36**(8), 1419–1425 (2015)
7. Goceri, E.: Medical image data augmentation: techniques, comparisons and interpretations. Artificial intelligence review **56**(11), 12561–12605 (2023)
8. Goni, M.R., Ruhaiyem, N.I.R., Mustapha, M., Achuthan, A., Nassir, C.M.N.C.M.: Brain vessel segmentation using deep learning—a review. IEEE access **10**, 111322–111336 (2022)
9. Huang, W., Gao, W., Hou, C., Zhang, X., Wang, X., Zhang, J.: Simultaneous vessel segmentation and unenhanced prediction using self-supervised dual-task learning in 3D CTA (SVSUP). Computer Methods and Programs in Biomedicine **224**, 107001 (2022). https://doi.org/10.1016/j.cmpb.2022.107001, iSBN: 0324088302
10. Isensee, F., Wald, T., Ulrich, C., Baumgartner, M., Roy, S., Maier-Hein, K., Jaeger, P.F.: nnU-Net revisited: a call for rigorous validation in 3D medical image segmentation (2024)
11. Isensee, F., Jaeger, P.F., Kohl, S.A., Petersen, J., Maier-Hein, K.H.: nnU-Net: a self-configuring method for deep learning-based biomedical image segmentation. Nature Methods **18**(2), 203–211 (2021). https://doi.org/10.1038/s41592-020-01008-z, http://dx.doi.org/10.1038/s41592-020-01008-z
12. Leng, X., Fang, H., Leung, T.W., Mao, C., Miao, Z., Liu, L., Wong, K.S., Liebeskind, D.S.: Impact of collaterals on the efficacy and safety of endovascular treatment in acute ischaemic stroke: A systematic review and meta-analysis. Journal of Neurology, Neurosurgery and Psychiatry **87**(5), 537–544 (2016). https://doi.org/10.1136/jnnp-2015-310965
13. Meijs, M., Manniesing, R.: Artery and vein segmentation of the cerebral vasculature in 4D CT using a 3D fully convolutional neural network (February 2018), 61 (2018). https://doi.org/10.1117/12.2292974, iSBN: 9781510616394
14. Meijs, M., Patel, A., van de Leemput, S.C., Prokop, M., van Dijk, E.J., de Leeuw, F.E., Meijer, F.J., van Ginneken, B., Manniesing, R.: Robust segmentation of the full cerebral vasculature in 4D CT of suspected stroke patients. Scientific reports **7**(1), 15622 (2017)
15. Pai, S., Hadzic, I., Bontempi, D., Bressem, K., Kann, B.H., Fedorov, A., Mak, R.H., Aerts, H.J.: Vision foundation models for computed tomography. arXiv preprint arXiv:2501.09001 (2025)
16. Roy, S., Koehler, G., Ulrich, C., Baumgartner, M., Petersen, J., Isensee, F., Jaeger, P.F., Maier-Hein, K.H.: Mednext: transformer-driven scaling of convnets for medical image segmentation. In: International conference on medical image computing and computer-assisted intervention. pp. 405–415. Springer (2023)
17. Su, J., Wolff, L., Van Es, A.C., Van Zwam, W., Majoie, C., Dippel, D.W., Van Der Lugt, A., Niessen, W.J., Van Walsum, T.: Automatic Collateral Scoring from 3D CTA Images. IEEE Transactions on Medical Imaging **39**(6), 2190–2200 (2020). https://doi.org/10.1109/TMI.2020.2966921
18. Tetteh, G., Efremov, V., Forkert, N.D., Schneider, M., Kirschke, J., Weber, B., Zimmer, C., Piraud, M., Menze, B.H.: DeepVesselNet: Vessel Segmentation, Centerline Prediction, and Bifurcation Detection in 3-D Angiographic Volumes pp. 1–13 (2018), http://arxiv.org/abs/1803.09340, arXiv: 1803.09340

19. van Voorst, H., Su, J., Konduri, P.R., Majoie, C.B., Roos, Y.B., Emmer, B.J., Marquering, H.A., de Vos, B.D., Caan, M.W., Išgum, I., others: Deep generative models for vessel segmentation in CT angiography of the brain. Computers in Biology and Medicine **202**, 111432 (2026)
20. de Vos, V., Timmins, K.M., van der Schaaf, I.C., Ruigrok, Y., Velthuis, B.K., Kuijf, H.J.: Automatic cerebral vessel extraction in TOF-MRA using deep learning. In: Medical Imaging 2021: Image Processing. vol. 11596, pp. 651–660. SPIE (2021)
21. Wang, H., Guo, S., Ye, J., Deng, Z., Cheng, J., Li, T., Chen, J., Su, Y., Huang, Z., Shen, Y., others: SAM-Med3D: a vision foundation model for general-purpose segmentation on volumetric medical images. IEEE Transactions on Neural Networks and Learning Systems (2025)
22. Wasserthal, J., Breit, H.C., Meyer, M.T., Pradella, M., Hinck, D., Sauter, A.W., Heye, T., Boll, D.T., Cyriac, J., Yang, S., others: TotalSegmentator: robust segmentation of 104 anatomic structures in CT images. Radiology: Artificial Intelligence **5**(5), e230024 (2023)
23. Wittmann, B., Wattenberg, Y., Amiranashvili, T., Shit, S., Menze, B.: vesselfm: A foundation model for universal 3d blood vessel segmentation. In: Proceedings of the IEEE/CVF Conference on Computer Vision and Pattern Recognition. pp. 20874–20884 (2025)
24. Wolff, L., Su, J., Van Loon, D., van Es, A., van Doormaal, P.J., Majoie, C., van Zwam, W., Dippel, D., van der Lugt, A., van Walsum, T., others: Inter-rater reliability for assessing intracranial collaterals in patients with acute ischemic stroke: comparing 29 raters and an artificial intelligence-based software. Neuroradiology **64**(12), 2277–2284 (2022)
25. Wouters, A., Seners, P., Yuen, N., Mlynash, M., Heit, J.J., Kemp, S., Demeestere, J., Christensen, S., Albers, G.W., Lemmens, R., others: Clinical and Imaging Features Associated With Fast Infarct Growth During Interhospital Transfers of Patients With Large Vessel Occlusions. Neurology **103**(6), e209814 (2024)
26. Yang, K., Musio, F., Ma, Y., Juchler, N., Paetzold, J.C., Al-Maskari, R., Höher, L., Li, H.B., Hamamci, I.E., Sekuboyina, A., others: Benchmarking the cow with the topcow challenge: Topology-aware anatomical segmentation of the circle of willis for cta and mra. ArXiv pp. arXiv–2312 (2025)